NANO LETTERS

pubs.acs.org/NanoLett

Ultrahigh Responsivity Visible and Infrared Detection Using Silicon Nanowire Phototransistors

Arthur Zhang,*,† Hongkwon Kim,† James Cheng, and Yu-Hwa Lo

Department of Electrical and Computer Engineering, Jacobs School of Engineering, University of California, San Diego, 9500 Gilman Drive, La Jolla, California 92093-0409

ABSTRACT Nanowire photodetectors can perform exceptionally well due to their unique properties arising from the nanowire geometry. Here we report on the phenomenal responsivity and extended spectral range of scalable, vertically etched, silicon nanowire photodetector arrays defined by nanoimprint lithography. The high internal gain in these devices allows for detection at below room temperatures of subfemtowatt per micrometer visible illumination and picowatt infrared illumination resulting from band to surface state generation.

KEYWORDS Silicon, nanowire, photodetector, visible, infrared

Silicon is widely used for photodetection at visible wavelengths in imager arrays. However, with the continued scaling of pixel density, the sensitivity of traditional devices has decreased as most of the pixel is taken over by amplification circuitry, reducing the photosensitive area. To continue increasing pixel density while maintaining high sensitivity, detectors with large enough intrinsic gain to bypass the need for external amplification are required. Vertical silicon nanowire arrays are particularly attractive in this area due to their extremely high intrinsic gain, long interaction length allowing for waveguiding effects to achieve quantum efficiencies above their physical fill factor, and ability to extend a substantial responsivity into the infrared spectrum not seen in bulk or thin film devices.[1−4] In this work we demonstrate the high responsivity achievable in vertically etched silicon nanowire phototransistors to both visible and infrared light. The detectors show a phenomenal response down to subfemtowatt visible and picowatt infrared illumination at below room temperatures.

Recent studies on both chemical vapor deposition grown[5−7] and etched[8−10] silicon nanowire photodetectors have begun to show the properties of these devices. The behavior of nanowire devices is strongly dependent on the surface effects due to their large surface to volume ratio.[11−17] In silicon nanowires, these effects lead to a phototransistive process, which results in a very high responsivity and increased spectral range. The physical mechanisms for the observed phototransistive gain are elucidated through mathematical modeling done previously[18] and numerical simulations using Silvaco. Our simulations consider a uniformly doped p-type silicon nanowire with 100 nm radius and 1 μm length with uniform illumination from the side (Figure 1a). Surface states are distributed along the band gap of Si at 0.4 eV above the valence band for donor states and below the conduction band for acceptor states as Gaussian distributions following a general model of the silicon surface.[19,20] Due to the larger number of donor states than acceptor states at the silicon surface causing surface Fermi pinning at 1/3 Eg above the valence band, the phototransistive effect is larger in p-type silicon and is thus the focus of our investigation. Ohmic contacts to the ends of the nanowire are used to bias the device at 1 V and a pseudo-three-dimensional simulation is performed by taking a radial slice of the structure and integrating around the body of the nanowire. The midgap electronic states at the silicon surface result in the trapping of majority carriers and surface depletion (Figure 1b) that causes band bending and a radial "gate" field (Figure 1c). Due to the gate field, photogenerated electrons are swept to the surface, where they recombine with trapped holes, in effect modulating the gate field, while holes are confined to the center of the nanowire. This process can greatly extend the lifetime of holes, which leads to a very high internal gain expressed as $G = \tau_l/\tau_t$ where τ_l is the hole lifetime and τ_t is the hole transit time.

To realize these devices, arrays of vertical silicon nanowires were fabricated. Vertically etched nanowire devices have the advantage of allowing for precise control over placement, geometry, and number. Epi silicon substrates with a layer structure consisting of a 0.3 μm p^+ source, 4 μm p^- device layer, and p^+ drain substrate, were patterned with Ni dots 200 nm in diameter and 1 μm in pitch using e-beam or nanoimprint lithography (Figure 2a). A doping of 10^{15} cm^{-3} was chosen for the device layer to allow for the nanowire to be fully depleted by surface states. Devices

* Corresponding author, ayzhang@ucsd.edu.

† These authors contributed equally in this work.

Received for review: 02/22/2010
Published on Web: 05/14/2010

DOI: 10.1021/nl1006432 | *Nano Lett.* **2010,** *10,* 2117–2120

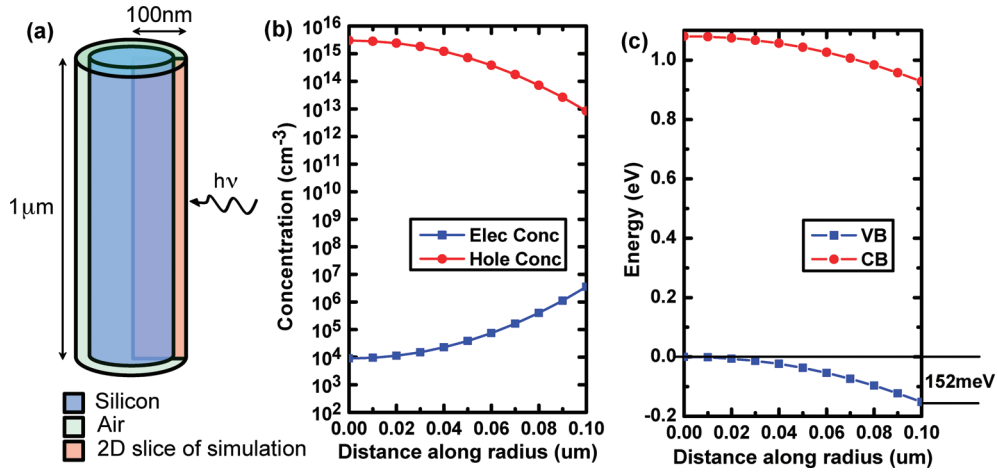

FIGURE 1. Numerical simulation of a silicon nanowire phototransistor. (a) Diagram of structure simulated with uniformly doped p-type silicon (blue) surrounded by air (green). Surface states are defined at the silicon/air interface and light is input from the side. Pseudo-three-dimensional simulation is performed by taking a radial slice (pink) and integrating around the nanowire. (b) Hole (red circles) and electron (blue squares) concentrations along the nanowire radius from center to surface for donor surface state concentration Ngd = 5×10^{10} cm^{-2} and doping Na = 4×10^{16} cm^{-3} showing a fully depleted nanowire caused by surface depletion. (c) Valence (blue squares) and conduction (red circles) band diagram (with same conditions as (b)) showing radial band bending caused by surface depletion.

formed using nanoimprint lithography are able to produce a very uniformly ordered array of wires that is easily scalable and low in fabrication cost and time. The nanowires are formed through RIE/ICP dry etching with C_4F_8 and SF_6 gases using the Ni as an etch mask and self-aligned contact and subsequently annealed at 650 °C to form NiSi at the top contact (Figure 2b). The nanowires are then embedded in polyimide, the tips exposed using O_2 plasma, and a transparent ITO contact patterned on top of the photoactive region. Final Ti/Au contacts are then patterned away from the active area (Figure 2c). Direct current measurements on these devices were performed in a low vacuum cryostat chamber with devices mounted on a temperature-regulated coldfinger and characterized with a parameter analyzer.

An important limiting factor in device responsivity is the generation/recombination (1/*f*) noise and shot noise, both proportional to the square root of the dark current, which can obscure a very small optical signal. Our nanowire devices are normally depleted by the surface states, dramatically decreasing the dark current and associated noise. Thus the dark current in these devices is limited by the thermionic emission of carriers from the p^+ source into the depleted nanowire channel like that of a nanowire transistor in the subthreshold regime. Figure 3a shows the dark current behavior with temperature at various total applied bias. The dark current follows an exponential behavior with inverse temperature as expected of thermionic emission. The energy needed for thermal carriers to be generated can be found by the current−temperature dependence as

$$I_{\mathrm{dark}} \sim \exp\left[\frac{q}{kT}\left(\frac{V_{\mathrm{B}}}{n} - \phi_{\mathrm{B}}\right)\right] \qquad (1)$$

where ϕ_B is the barrier height, kT/q is the thermal voltage, V_B is the bias across the barrier, and n is the ideality factor. The barrier height for emission of holes from the p^+ source can be found by taking the slope of the semilog plot and is found to be 0.15 eV. As seen from the plot, the height of the barrier is unaffected by the total bias, as most of the applied bias drops across the high impedance depleted nanowire channel.

A very promising characteristic of our silicon nanowire phototransistors is their very sensitive behavior to both above-band-gap absorption of visible light, and sub-band-gap absorption of infrared light due to its high internal gain mechanism and enhanced absorption efficiency. Although the actual photosensitive area of a vertical nanowire pixel can be very small, only 3% in our structure, the high refractive index contrast between the semiconductor and surrounding medium causes light incident around the nanowire to be guided into the device.[14] Figure 3b shows the photocurrent of devices illuminated at various intensities using 635 and 1550 nm lasers at various temperatures. Under visible illumination, the device shows a very high responsivity with detection levels of less than 0.1 fW/μm^2 incident power per nanowire, which is at the limit of background level illumination in our setup. This incredible sensitivity is possible due to the low dark current noise and high internal gain inherent in the nanowire structure. The device also shows responsivity to 1550 nm infrared illumination greatly beyond what is possible in band to band absorption in bulk, single-crystalline silicon. In bulk silicon, infrared absorption resulting from band to surface state transitions is negligible due to the small surface to volume ratio. However, in nanowire devices the surface to volume ratio can be high enough to allow for a substantial responsivity to infrared light. The observed infrared response of our detector is orders of magnitude higher than one would expect by considering only the absorption coefficient of bulk silicon at this wavelength[21] and shows a detectable response

DOI: 10.1021/nl1006432 | *Nano Lett.* **2010,** *10,* 2117–2120

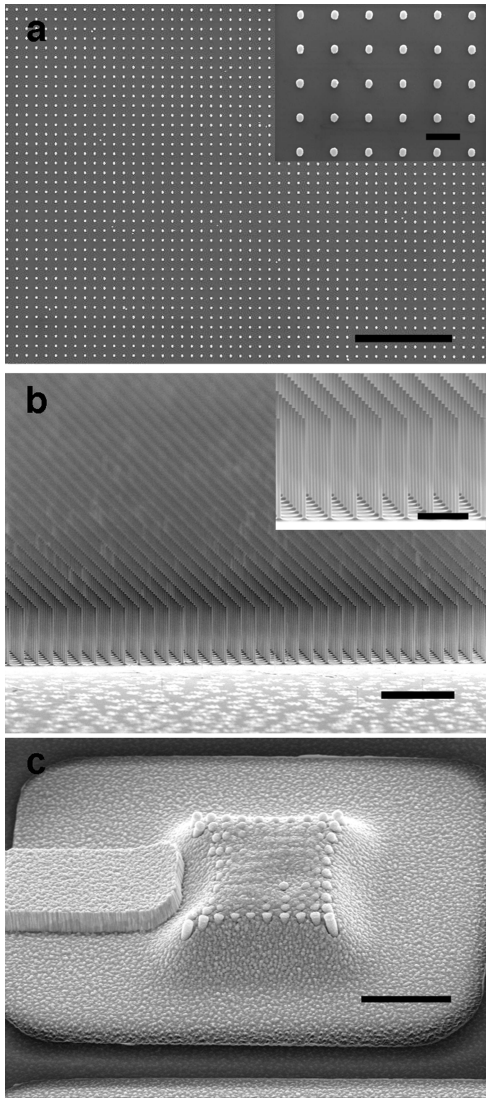

FIGURE 2. SEM images of fabricated devices. (a) Large area and zoomed in (inset) views of samples fabricated using nanoimprint lithography after Ni etch mask and contact dot patterning (scale bars are 10 and 1 μm for inset). (b) Large area and zoomed in (inset) views after Si nanowire etching to 4 μm (scale bars are 5 and 2 μm for inset). (c) Finished 100 nanowire array device showing nanowires embedded in polyimide with top ITO contact, and Ti/Au metal finger leading to a contact pad not shown (scale bar is 5 μm). Diameter and pitch are 200 nm and 1 μm, respectively, for all images.

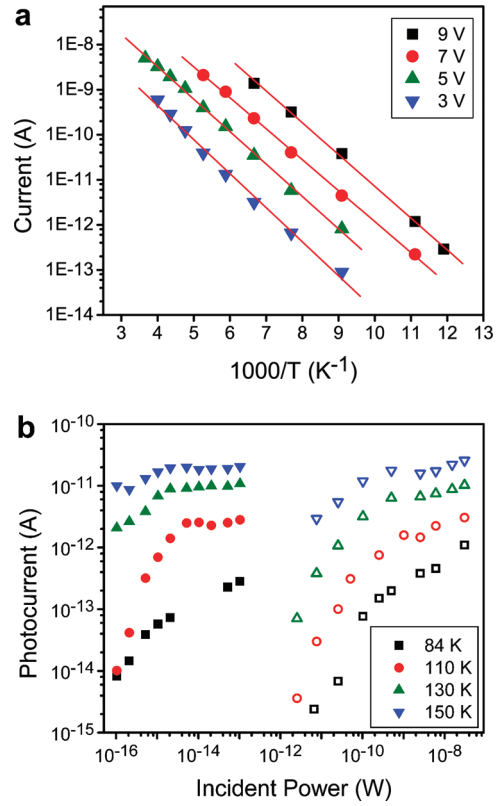

FIGURE 3. Measurement results of a silicon nanowire phototransistor array normalized to a single wire. Nanowires are 200 nm in diameter and 4 μm in length with 1 μm pitch. (a) Dark current vs temperature at different biases (black squares, 9 V; red circles, 7 V; green upward triangle, 5 V; blue downward triangle, 3 V) showing an energy barrier of ~0.15 eV for holes between the source and nanowire as a transistor in subthreshold regime. (b) Photocurrent under various illumination levels of visible (solid symbols) and IR (hollow symbols) light for device biased at 5 V measured at different temperatures (black squares, 84 K; red circles, 110 K; green upward triangle, 130 K; blue downward triangle, 150 K).

at incident illumination levels on the order of 1 pW per wire. The 4 orders of magnitude reduction in responsivity compared to visible illumination is partly due to the decreased absorption enhancement due to the waveguiding effect at longer wavelengths (see Supporting Information on spectral response) and partly due to the lower absorption cross section from the fewer number of states available for band to surface generation compared to band to band transitions. The photocurrents in each case decrease with decreasing temperature due to the injection barrier at the p^+ source. As the temperature decreases, the carriers have less thermal energy to overcome the barrier, which decreases the photocurrent.

The device performance can be expressed in terms of the responsivity, which is directly related to the internal gain of the device and is plotted against incident optical power in Figure 4 for both visible and infrared illumination. The peak responsivity of 10^5 A/W observed for visible illumination and 10^2 A/W for infrared illumination is much greater than similar nanowire devices[6−8,10] or conventional silicon photodiodes with a typical responsivity below 1 A/W. An important characteristic of these devices is the decay of the responsivity at higher optical power. As the light intensity increases, the number of electron hole pairs generated in the nanowire increasingly deviates from thermal equilibrium values. The increasing number of holes in the center of the wire lowers the potential barrier confining the holes, which decreases the lifetime of holes and therefore the gain and responsivity. This effect parallels automatic gain control circuits, which allows for a much larger dynamic range, making these devices excellent candidates for applications requiring either very low light intensity detection or normal photodetector arrays. The gain in these devices is also seen

DOI: 10.1021/nl1006432 | Nano Lett. 2010, 10, 2117–2120

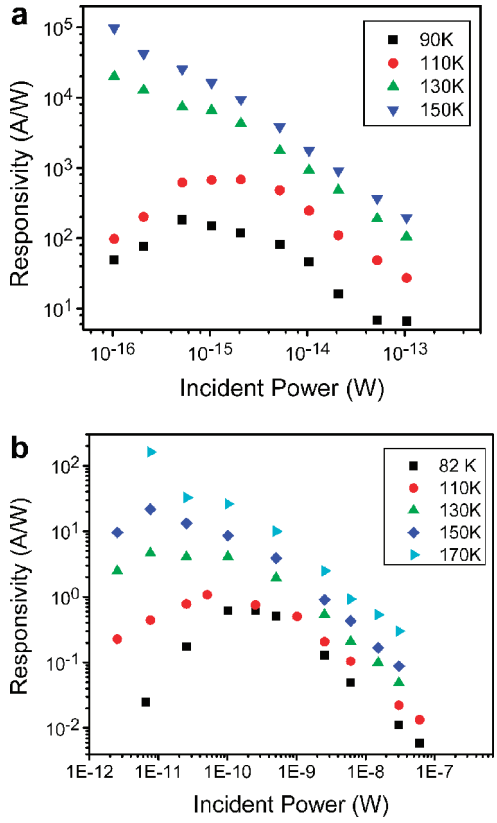

FIGURE 4. Responsivity vs laser power incident on a silicon nanowire phototransistor array at various temperatures for (a) visible illumination at 5 V bias (black squares, 90 K; red circles, 110 K; green upward triangle, 130 K; blue downward triangle, 150 K) and (b) IR illumination at 9 V bias (black squares, 82 K; red circles, 110 K; green upward triangle, 130 K; blue diamond, 150 K; teal right-pointing triangle, 170 K). Incident power is normalized to a 1 × 1 μm^2 area around a single wire. Nanowires are 200 nm in diameter and 4 μm in length with 1 μm pitch.

to increase with increasing temperature. As the temperature is lowered, the barrier for hole capture at the surface states effectively increases, which increases the lifetime and gain. However, the barrier for hole injection at the contacts also increases with decreasing temperature, which lowers the photocurrent and gain. This effect dominates the behavior of the device but becomes negligible at high enough temperatures allowing for holes with enough thermal energy to overcome this barrier. Thus the increase in gain is seen to saturate between 150 and 170 K. Although the level of gain is maintained with further increasing temperature, the detection of such small signals is increasingly more difficult as the dark current and its associated noise eventually overwhelm the photoresponse. Thus, for maximum responsivity, an operating temperature to balance these two factors must be considered.

A vertical single-crystalline silicon nanowire phototransistor has been demonstrated and shown to be able to detect subfemtowatts of visible light and picowatts of infrared (1550 nm) light at below room temperature. Fabrication of devices using nanoimprint lithography allows for very uniform large area arrays to be patterned quickly and cost-effectively. Sub-bandgap response is observable in these devices due to band to surface photogeneration of carriers, possible only in these nanostructures with their large enough surface to volume ratio and surface state density. The broad spectral response and high responsivity lend these devices toward a myriad of applications in communications, imaging, and sensing.

Acknowledgment. This work was partially supported by Agiltron, Inc., through an SBIR Phase-II contract with the Department of Energy. The authors thank Dr. Yisi (Lewis) Liu of Agiltron for providing e-beam lithographic samples and UCSD Nano3 staff for providing an excellent facility and services for nanoscaled device fabrication. A.Z. is grateful for support from a National Science Foundation Graduate Research Fellowship. H.K. is grateful for support from Samsung SMD.

Supporting Information Available. Simulations and experimental results of absorption enhancement dependence on wavelength. This material is available free of charge via the Internet at http://pubs.acs.org.

REFERENCES AND NOTES

(1) Colace, L.; Sorianello, V.; Balbi, M.; Assanto, G. *Appl. Phys. Lett.* **2007**, *91*, No. 021107.
(2) Crouch, C. H.; Carey, J. E.; Warrender, J. M.; Aziz, M. J.; Mazur, E.; Genin, F. Y. *Appl. Phys. Lett.* **2004**, *84*, 1850–1852.
(3) Schmid, P. E. *Phys. Rev. B* **1981**, *23*, 5531–5536.
(4) Vivien, L.; Rouviere, M.; Fedeli, J.-M.; Marris-Morini, D.; Damlencourt, J.-F.; Mangeney, J.; Crozat, P.; El Melhaoui, L.; Cassan, E.; Le Roux, X.; Pascal, D.; Laval, S. *Opt. Express* **2007**, *15*, 9843–9848.
(5) Ahn, Y.; Dunning, J.; Park, J. *Nano Lett.* **2005**, *5*, 1367–1370.
(6) Kim, K.-H.; Keem, K.; Jeong, D.-Y.; Min, B.; Cho, K.; Kim, H.; Moon, B.-M.; Noh, T.; Park, J.; Suh, M.; Kim, S. *Jpn. J. Appl. Phys.* **2006**, *45*, 4265–4269.
(7) Servati, P.; Colli, A.; Hofmann, S.; Fu, Y. Q.; Beecher, P.; Durrani, Z. A. K.; Ferrari, A. C.; Flewitt, A. J.; Robertson, J.; Milne, W. I. *Physica E* **2007**, *38*, 64–66.
(8) Francinelli, A.; Tonneau, D.; Cleiment, N.; Abed, H.; Jandard, F.; Nitsche, S.; Dallaporta, H.; Safarov, V.; Gautier, J. *Appl. Phys. Lett.* **2004**, *85*, 5272.
(9) Choi, H. G.; Choi, Y.-S.; Jo, Y. C.; Kim, H. *Microprocesses and Nanotechnology Conference*; IEEE: New York, 2003; pp 296−297.
(10) Park, J.-H.; Seo, S.-H.; Wang, I.-S.; Yoon, H.-J.; Shin, J.-K.; Choi, P.; Jo, Y.-C.; Kim, H. *Jpn. J. Appl. Phys.* **2004**, *43*, 2050–2053.
(11) Calarco, R.; Marso, M.; Richter, T.; Aykanat, A. I.; Meijers, R.; Hart, A. V.; Stoica, T.; Luth, H. *Nano Lett.* **2005**, *5*, 981–984.
(12) Chen, R.-S.; Chen, H.-Y.; Lu, C.-Y.; Chen, K.-H.; Chen, C.-P.; Chen, L.-C.; Yang, Y.-J. *Appl. Phys. Lett.* **2007**, *91*, 223106.
(13) Soci, C.; Zhang, A.; Xiang, B.; Dayeh, S. A.; Aplin, D. P. R.; Park, J.; Bao, X. Y.; Lo, Y.-H.; Wang, D. *Nano Lett.* **2007**, *7*, 1003–1009.
(14) Zhang, A.; You, S.; Soci, C.; Liu, Y.; Wang, D.; Lo, Y.-H. *Appl. Phys. Lett.* **2008**, *93*, 121110.
(15) Ingole, S.; Manandhar, P.; Chikkannanavar, S. B.; Akhadov, E. A.; Picraux, S. T. *IEEE Trans. Electron Devices* **2008**, *55*, 2931–2938.
(16) Vaurette, F.; Nys, J. P.; Deresmes, D.; Grandidier, B.; Stievenard, D. *J. Vac. Sci. Technol., B* **2008**, *26*, 945–948.
(17) Ng, M.-F.; Shen, L.; Zhou, L.; Yang, S.-W.; Tan, V. B. C. *Nano Lett.* **2008**, *8*, 3662–3667.
(18) Soci, C.; Zhang, A.; Bao, X.-Y.; Kim, H.; Lo, Y.-H.; Wang, D. *J. Nanosci. Nanotechnol.* **2010**, *10*, 1430–1449.
(19) Flietner, H. *Surf. Sci.* **1988**, *200*, 463–471.
(20) Olibet, S.; Vallat-Sauvain, E.; Ballif, C. *Phys. Rev. B* **2007**, *76*, No. 035326.
(21) Green, M. A. *Sol. Energy Mater. Sol. Cells* **2008**, *92*, 1305–1310.

DOI: 10.1021/nl1006432 | *Nano Lett.* **2010,** *10,* 2117–2120